Faulting and hydration of the Juan de Fuca plate system

Mladen R. Nedimović[1,3], DelWayne R. Bohnenstiehl[2,3], Suzanne M. Carbotte[3], J. Pablo Canales[4] and Robert P. Dziak[5]

[1]*Department of Earth Sciences, Dalhousie University, Room 3006, Life Sciences Centre, Halifax, NS, B3H 4J1, Canada*

[2]*Department of Marine, Earth and Atmospheric Sciences, North Carolina State University, Campus Box 8208, Raleigh, NC 27695, USA*

[3]*Lamont-Doherty Earth Observatory of Columbia University, 61 Route 9W, P. O. Box 1000, Palisades, NY 10964-8000, USA*

[4]*Department of Geology and Geophysics, MS#24, Woods Hole Oceanographic Institution, 360 Woods Hole Rd., Woods Hole, MA 02543, USA*

[5]*Hatfield Marine Science Center, Oregon State University and NOAA, 2030 Marine Science Dr., Newport, OR 97365, USA*

Corresponding author

M. R. Nedimović

Department of Earth Sciences

Life Sciences Centre

Dalhousie University

Edzell Castle Circle, Halifax

NS, B3H 4J1, Canada

Telephone: 902-494-4524

Fax: 902-494-6889

E-mail: mladen@dal.ca

Abstract

Multichannel seismic observations provide the first direct images of crustal scale normal faults within the Juan de Fuca plate system and indicate that brittle deformation extends up to ~200 km seaward of the Cascadia trench. Within the sedimentary layering steeply dipping faults are identified by stratigraphic offsets, with maximum throws of 110±10 m found near the trench. Fault throws diminish both upsection and seaward from the trench. Long-term throw rates are estimated to be 13±2 mm/kyr. Faulted offsets within the sedimentary layering are typically linked to larger offset scarps in the basement topography, suggesting reactivation of the normal fault systems formed at the spreading center. Imaged reflections within the gabbroic igneous crust indicate swallowing fault dips at depth. These reflections require local alteration to produce an impedance contrast, indicating that the imaged fault structures provide pathways for fluid transport and hydration. As the depth extent of imaged faulting within this young and sediment insulated oceanic plate is primarily limited to approximately Moho depths, fault-controlled hydration appears to be largely restricted to crustal levels. If dehydration embrittlement is an important mechanism for triggering intermediate-depth earthquakes within the subducting slab, then the limited occurrence rate and magnitude of intraslab seismicity at the Cascadia margin may in part be explained by the limited amount of water imbedded into the uppermost oceanic mantle prior to subduction. The distribution of submarine earthquakes within the Juan de Fuca plate system indicates that propagator wake areas are likely to be more faulted and therefore more hydrated than other parts of this plate system. However, being largely restricted to crustal levels, this localized increase in hydration generally does not appear to have a measurable effect on the intraslab seismicity along most of the subducted propagator wakes at the Cascadia margin.

Keywords: Juan de Fuca plate system; seismic reflection imaging; faulting; hydration; earthquakes.

1. Introduction

Oceanic plates carry physically and chemically bound water into subduction zones (e.g., Peacock, 1990; Meade and Jeanloz, 1991; Moore and Vrolijk, 1992; Ranero et al., 2003). As the subducting oceanic plates descend, and the pressure and temperature rise with the increasing depth, the water stored in the plates is gradually released through a series of dehydration reactions (e.g., Meade and Jeanloz, 1991; Kirby et al., 1996; Peacock, 2001, Hacker et al., 2003a,b). This free water is believed to strongly affect a number of processes important to natural hazard studies. The released water promotes partial melting responsible for arc magmatism (Tatsumi and Eggins, 1995; Kirby et al., 1996), can affect the mechanical characteristics of an interplate interface (Shipley et al., 1994; Nedimović et al., 2003a; Kodaira et al., 2004), and induces intraslab earthquakes at intermediate depths (~50-300 km) (Raleigh and Paterson, 1965; Meade and Jeanloz, 1991; Kirby et al., 1996).

Significant effort has therefore been directed toward understanding dehydration processes during subduction, with particular emphasis on the influence these processes may have on the depth-distribution of intraslab seismicity (Meade and Jeanloz, 1991; Peacock, 2001; Hacker et al, 2003a,b; Jung et al., 2004). To fully evaluate the importance of slab dehydration, however, it also is necessary to constrain the amount of water bound in the slab when it is subducted at the trench (Ranero et al., 2003). We focus our effort on determining the penetration depth and relative volume extent of oceanic slab hydration offshore Cascadia margin. For this purpose, we process ~1500 km of ridge-flank multi-channel seismic (MCS) data collected in 2002 during the EW0207 cruise and compile a database of seismic reflection profiles from all earlier crustal scale MCS surveys (streamers 2.4 km or longer) across the Juan de Fuca plate system. The spatial distribution of the MCS lines examined is shown in Fig. 1, along with magnetic isochrones (Wilson, 2002) and the locations of Cascadia margin earthquakes believed to

be spatially restricted to the Juan de Fuca plate and subducting slab (Fox et al., 1994; McCrory et al., 2004).

2. Study area

The study area shown in Fig. 1, located offshore western North America, encompasses the Juan de Fuca ridge and plate system (Explorer, Juan de Fuca and Gorda ridges and plates), Cascadia deformation front, Nootka fault, and Sovanco and Blanco fracture zones. The Juan de Fuca ridge system, a NNE-oriented intermediate-rate spreading center, is located at the boundary between the Pacific plate and the Juan de Fuca plate system. The full spreading rate along the Juan de Fuca ridge is 56 mm/yr, and 56 mm/yr and less along the Explorer and Gorda ridges (e.g., Wilson, 1993). The Cascadia deformation front marks the surface trace of the interface between the Juan de Fuca and North America plates. The Nootka fault is the boundary between the Explorer and the Juan de Fuca plates, and Blanco and Sovanco fracture zones separate parts of the Juan de Fuca plate system from the Pacific plate.

Both the western and eastern flanks of the Juan de Fuca ridge system are crossed by propagator wakes but otherwise show prominent differences indicating that they are evolving in a markedly different way due to distinct sedimentary and volcanic histories. Seamounts, which are found primarily on the Pacific plate, occur as isolated edifices and in chains, several of which lie close to and intersect the Juan de Fuca ridge axis (Davis and Karsten, 1986). Sediments covering the eastern Juan de Fuca ridge flank are up to a few kilometers thick at the northern Cascadia subduction deformation front and thin toward the ridge axis and southward away from the dominant source of terrigenous sediment (Nedimović et al., 2008). The western Juan de Fuca ridge flank is more sparsely sedimented, although sediment cover generally increases to the north where significant sediment accumulation is confined to mini-basins between large basement outcrops. The

enhanced accumulation of sediment on the eastern flank is in large part caused by the morphology of the Juan de Fuca ridge, with its cooling and subsiding flanks forming basin-like depositional environments and its elevated axial region acting as a barrier that inhibits the transport of terrigenous sediment to the western flank.

3. Reflection imaging

Summary information and corresponding references that describe the MCS data used in this study are provided in Table 1. The prestack processing strategy adopted for the EW0207 MCS data consisted of: Standard straight-line CMP bin geometry; F-K and bandpass (2-7-100-125 Hz) filtering to remove the low frequency cable noise; amplitude correction for geometrical spreading; surface consistent minimum phase predictive deconvolution to balance the spectrum and remove short period multiples; surface consistent amplitude correction to correct for anomalous shot and receiver-group amplitudes not related to wave propagation; trace editing; velocity analysis using the velocity spectrum method; normal moveout and dip moveout corrections to align signal for stacking; and CMP mute to remove overly stretched data. Crossdip moveout correction (Nedimović et al., 2003b) was not required because streamer feathering was small (<10°) and structural crossdip negligible. The prepared prestack data, with and without the automatic gain control, were then stacked (averaged). The poststack processing included seafloor mute, primary multiple mute to reduce migration noise, bandpass filtering (2-7-100-125 Hz), and time migration to collapse diffractions and position the recorded reflection events to their true subsurface locations. To improve imaging within the oceanic plate below the upper crust, the late travel time data were additionally bandpass filtered at 2-7-20-40 Hz and mildly coherency filtered.

Analyzed seismic images from field programs other than the 2002 Juan de Fuca cruise were formed earlier by other researchers in a similar way as described for the

EW0207 cruise. Specific details about the processing stream are provided in Calvert and Clowes (1991) for the 1985 Frontier Geoscience project, in Calvert (1996) for the 1989 ODP Leg 146 site survey offshore Vancouver Island, in MacKay et al. (1992) for the 1989 ODP Leg 146 site survey offshore Oregon, in Flueh et al. (1998) for the 1996 Orwell project, and in Gulick et al. (1998) for the 1994 Mendocino Triple Junction experiment. The 1994 Gorda Rise and Cape Blanco data were processed only to near-offset brute stacks (Brocher et al., 1995; *http://www.ig.utexas.edu/sdc/cruise.php?cruiseIn=ew9413*). This processing included: trace edit, amplitude recovery, bandpass filter, CMP sort, normal moveout, stretch mute and stack. From the various survey campaigns described here only some of the Orwell project profile data, although collected using the shortest streamer (2.4 km) with the smallest number of channels (48), were prestack depth processed (Flueh et al., 1998).

4. Characterization of faulting

Analysis of the compiled database of seismic reflection images (Fig. 1) resulted in an outline of the Juan de Fuca plate region of extension or transtension, where normal faulting is observed (Fig.1). The faulting appears nearest to the ridge axis at the northern end of the Juan de Fuca plate but the width of the faulted zone seems to increase southward along the trench, reaching a maximum of over 200 km near the Blanco fracture zone. Both Explorer and Gorda plates experience deformation throughout, as indicated by the seismicity (Fig. 1). However, seismic reflection constraints on the extent of normal faulting in these two areas are rather limited due to the lack of profile coverage or insufficient image resolution.

In Fig. 2 we show for the first time a reflection image of faults within the Juan de Fuca plate system that extend all the way through the sediments and crust to about the Moho discontinuity. The imaged faults are spatially tied to ridge-parallel fault structures

153 that represent pre-existing zones of weakness. Fault offsets gradually diminish up-section
154 with sediment age, suggesting growth faulting caused by repeated slip on basement
155 structures (Figs. 2 and 3). Our reflection image resolution permits identification of fault-
156 plane sections within the sediments with throws >2-3 m. This resolution estimate is
157 governed by the data sample rate (2 ms), sediment interval velocities (1550-3300 m/s),
158 and frequency content of the signal (from ~2 Hz to over 100 Hz). Therefore, based only
159 on the reflection images, we cannot conclude whether the lack of visible faulting within
160 the topmost sediments (Fig. 3) is due to the limited image resolution, or due to the
161 absence of recent dip-slip displacement on these structures.

162 To resolve this, we first estimate the maximum longterm fault-throw rates for the
163 study area and then compare them with the recent sedimentation rates. Maximum fault
164 throws of 110±10 m are observed offshore Oregon, just west from the trench along the
165 ODP Leg 146 line 8. The shortest distance seaward from this fault toward the onset of
166 faulting is 200±20 km, and the half spreading rate is 28 mm/yr (e.g., Wilson, 1993). This
167 information yields a maximum longterm throw rate of 15±2 mm/kyr. We also estimate
168 the same parameters along the 2002 Juan de Fuca survey transect 17-3-1 offshore
169 Vancouver Island/Olympic Peninsula that spatially coincides with the Endeavour
170 ODP/IODP drilling transect, and for which there is a wealth of information about the
171 sedimentation rates. Maximum identified throw along this profile is 20±2 m; trench
172 normal distance between the maximum throw fault and the seaward onset of faulting is
173 50±5 km; and the half spreading rate is also 28 mm/yr. These data yield a maximum
174 long-term throw rate of 11±2 mm/kyr. The two calculated long-term throw rates agree
175 within the error limits and combined give an average long-term throw rate for the imaged
176 normal faults along the Juan de Fuca plate of 13±2 mm/kyr. This long-term throw-rate
177 estimate is more than 25 times smaller than the rapid average sedimentation rate of ~336
178 mm/kyr obtained for the time-stratigraphic period A characterizing the past 90 kyr along

179 the Endeavour ODP/IODP drilling transect (Underwood et al., 2005). The topmost
180 sediments accumulated during the time-stratigraphic period A have an average thickness
181 of some 30 m while the estimated cumulative fault throw during this period is 1.17±0.18
182 m, less than the resolution threshold for our images. This suggests that plate-deforming
183 processes have remained active during most recent geologic time with the resulting
184 normal faulting displacing the whole sediment column.

185 Fault throws show no reversals in slip direction and gradually increase both
186 downsection, from younger to older sediments, and toward the trench with increasing
187 crustal age. Observations of compaction-induced sediment folding without faulting at
188 places where there are large offsets in the basement structure (e.g., Fig. 3 at ~125 km;
189 Fig. 4 at ~85 km; Figs. 5 and 6 at ~120 km) suggests that the sediment rupture is not
190 caused by compaction, but rather by movement of basement fault systems. Particularly
191 supportive of this interpretation is the Fig. 4 reflection image of the section of transect
192 17-3-1 showing significant sediment accumulation on the western Endeavour ridge flank.
193 Folding of sedimentary strata due to differential compaction over the rough igneous
194 basement is present throughout the mini-basins but no faulting can be observed despite
195 the large, up to a few hundred meters high steps in the basement structure. These mini-
196 basins extend to more than 110 km west from the Endeavour ridge axis, significantly
197 farther than the distance east from the Juan de Fuca ridge axis (55-110 km) at which the
198 seaward limit of faulting is observed on all transects (Figs. 1, 2, 3, 6). Moreover,
199 sediment thickness in the mini-basins over the western Endeavour ridge flank (Fig. 4) is
200 twice that on the eastern Endeavour flank at the seaward limit of faulting (Fig. 2), further
201 indicating that the faulting is caused by movement of basement fault systems and not
202 differential compaction. However, faulting in the sediments where there are only small
203 offsets in the basement implies that faulting does not in all cases occur at the pre-existing
204 planes of weakness formed at the Juan de Fuca ridge system.

205 The growth-fault interpretation is in general in agreement with the existing
206 lithospheric stress models for the Juan de Fuca plate system (Wang et al., 1997).
207 Nevertheless, the intraplate stress regime for the Juan de Fuca plate system is known to
208 be complex, with variable distribution of compressive and tensile stresses, and it is
209 possible that many of the described faults may have also experienced transcurrent
210 motion. Based on reflection images of the sediments (MacKay et al., 1992; Gulick et al.,
211 1998), and from earthquake studies and high-resolution images of the seafloor (Chaytor
212 et al., 2004), strike-slip and normal faulting have both been suggested for the Gorda and
213 southern part of the Juan de Fuca plate. Our images are 2D and sparsely distributed thus
214 providing no constraints on transcurrent motion along the imaged faults.

215 Crustal faulting within young oceanic plates is in most cases inferred from offsets
216 observed at the igneous basement or within the overlying sediments, as shown in Fig. 3.
217 Fig. 2 is exceptional because it shows reflections from the fault planes that can be
218 identified within the lower half of the image, or the lower two-thirds of the igneous
219 oceanic crust assuming average crustal velocities. The deep faulting projects to offsets in
220 the igneous basement and sediments indicating that the faults transect the whole crust.
221 This suggests that the imaged faults are listric—too steep to be imaged in the shallow-
222 most crust, and sloping gently enough to be imaged at greater depth.

223 Crustal reflections can potentially also be caused by varying mineralogical
224 content (e.g., of plagioclase) inherited from axial igneous processes; however, the
225 geometry of the boundary between crustal zones of different mineralogical content is
226 unlikely to both a) be identical to that caused by normal faulting and b) spatially correlate
227 with the position of basement scarps and faulting in the sediments. Furthermore, the
228 sharp changes in crustal mineralogical content needed to produce imageable reflections
229 are not common in nature, at least not in our study area where images of the oceanic crust

are void of any reflectivity excluding the top of the igneous crust and Moho events, and the small number of fault-related steeply dipping events discussed in this work.

The imaged fault reflections are not migration or other artefacts because their geometrical shape does not resemble that of migration 'smiles', they extend over a very long distance through the sections, and they project onto the displaced sediments. Moreover, the seismic sections formed using data collected during the 2002 Juan de Fuca cruise are of high signal-to-noise ratio (Nedimović et al., 2005) and are generally void of seismic noise that could be misinterpreted as fault reflections. Primary multiples are very strong and limit the depth to which the obtained images can be interpreted. In Fig. 2, primary multiples arrive at about 7 s two-way traveltime. We show this section to 6.4 s two-way traveltime because the deeper portion to 7 s is affected by primary multiples migration noise.

The observed fault reflections returning from within the mostly gabbroic oceanic crust and mostly peridotitic uppermost mantle are possible only if the rocks along the fault surfaces are altered to produce an acoustic impedance contrast. As these alteration products require the availability of seawater, this indicates that the extensional faults along the Juan de Fuca plate system are conduits for fluids and that their observed depth extent in the reflection images should constrain the local depth limit of plate hydration. The depth of imageable fault penetration correlates well with the 500-600 °C isotherm and is approximately coincident with the location of the Moho reflection (Fig. 2). At greater depths and therefore greater temperatures, serpentinization, the most important hydration mechanism for peridotites, becomes a marginal process (Ulmer and Trommsdorff, 1995). The lowest Juan de Fuca plate temperatures are expected along the Oregon Margin (8-10 Ma crust); however, due to the increasing accumulation of an insulating and heat producing sediment layer, thermal models predict that Moho temperatures will remain high (450-500° C) as the plate enters the trench (Hyndman and

Wang, 1993, 1995; Wang et al., 1995). Therefore, it appears that prior to subduction only the uppermost Juan de Fuca mantle can become hydrated by peridotite "corrosion" to serpentinite, despite the pervasive extensional faulting imaged seaward of the trench (Figs. 2 and 3).

After subduction, increased pressure may cause the antigorite stability region to initially increase as the slab starts to descend (e.g., Wada et al., 2008). Provided fault systems maintain permeability, free-water within the plate could facilitate additional and deeper serpentinization of the mantle rocks during this time. This process is expected to be common to all slabs; however, its extent cannot be assessed readily from reflection imaging. Dehydration occurs during later stages of subduction in response to slab warming.

5. Comparisons and implications

The only other convergent margin with both seismic reflection evidence for the depth extent of faulting and thermal modelling results is the Middle America subduction zone (Ranero et al., 2003; Harris and Wang, 2002). Normal faulting offshore Middle America margin covers a narrower swath of seafloor (~60 km) but is more pronounced than offshore Cascadia margin where the faulted area is wider (100-250 km). The width of the faulted area offshore Middle America appears consistent with the 40-75 km wide area estimated from lower resolution single-channel seismic and sidescan images from the outer-rise region of other subduction zones (e.g., Mason, 1991). The anomalously wide zone documented on the Juan de Fuca plate may indicate that the stress field within this small plate is not controlled solely by plate bending, but includes contributions from thermal contraction and basal shear, as well as ridge and transform push (Wang, 1997). Fault fabric inherited from crustal accretion at the ridge also has relatively little time to heal and may therefore be reactivated even under small differential stresses found at a

281 great distance from the trench. Alternatively, the faulting offshore Middle America
282 margin (and elsewhere) may start at a greater distance from the trench than observed, but
283 the combination of slower sedimentation rates and few available high quality MCS
284 reflection images makes it impossible to resolve faults with throws smaller than ~10-20
285 m with the existing data.

286 Faults are imaged to depths of ~6-7 km within the Juan de Fuca plate system.
287 Although there are currently no seismic reflection constraints on the depth extent of
288 faulting within the oldest portions of the plate near the Cascadia margin, thermal
289 modelling (Hyndman and Wang, 1993,1995; Wang et al., 1995) indicates that these
290 systems should extend no more than a few kilometers into slab mantle. At the Middle
291 America trench, however, faults are imaged to depths of ~20-22 km, some 15 km into the
292 upper mantle. Like at the Cascadia margin, the depth of imageable fault penetration at the
293 Middle America trench correlates well with the 500-600 °C isotherm from thermal
294 models. The Middle America outer-rise fault density gradually increases toward the
295 trench reaching ~8 faults per 5 km. Fault density at the Cascadia margin, although
296 variable, is comparatively low across the faulted area with ~1-2 faults per 5 km trench-
297 normal distance. While fault throws at the Middle America trench can reach ~500 m,
298 those adjacent to the Cascadia trench exhibit maximum offsets of only ~110 m. These
299 differences in fault density, fault throws, and imageable depth of fault penetration suggest
300 that the amount of water bound in the subducting slab at the Middle America trench is
301 significantly greater than that at the Cascadia margin. Specifically, the contribution from
302 serpentinized upper mantle rocks, which is equivalent to a 0.17-1.7 km-high column of
303 water per unit length at the Middle America trench (Ranero et al., 2003), appears to be
304 largely absent along Cascadia. This missing volume rivals the amount of water stored in
305 the igneous oceanic crust (Moore and Vrolijk, 1992).

306 Much attention has been given to the role of dehydration embrittlement in
307 triggering intermediate-depth earthquakes within the subducting slab and the localization
308 of these seismic events on pre-existing fault sets (Raleigh and Patterson, 1965; Yamasaki
309 and Seno, 2003; Hacker et al., 2003b). As shown in Fig. 1, intraslab seismicity at the
310 Cascadia margin is sparse and shallow (<~80-90 km), and focused in only a few areas—
311 the southern margin of the slab near the Mendocino triple junction, the eastern Olympic
312 peninsula region, and to a lesser extent the area beneath mid-western Vancouver Island
313 (Fig. 1). The largest recorded intraslab events occur in a small area offshore northern
314 California, have shallow hypocenters (<20 km depth), strike-slip mechanisms, and
315 moment magnitudes of up to ~7.3 (Wong, 2004). The largest intermediate-depth intraslab
316 earthquakes occur onshore across the northern Cascadia subduction zone. Their observed
317 maximum moment magnitudes are ~6.8 (April 23, 1949 Olympia and February 28, 2001
318 Nisqually earthquakes) (Malone, 2001; Rogers and Crosson, 2002). In the case of the
319 2001 Nisqually earthquake (slab age ~10 Ma at the time of subduction), waveform
320 analysis suggests that the rupture occurred on a steeply dipping plane that spanned the
321 lower oceanic crust and extended no more than 10 km into the subducted mantle (Kao et
322 al., 2008). This is consistent with the idea that as antigorite dehydration begins and fluids
323 migrate upward, the maximum depth extent of the embrittled mantle region is limited by
324 the original depth of hydration. By comparison, the maximum moment magnitude for
325 analogous, intermediate-depth events recorded at the Middle America margin, which is
326 characterized by abundant and deeper reaching (300 km) intermediate depth seismicity, is
327 nearly a full magnitude unit larger (Seno and Yoshida, 2004). For the largest recorded
328 event, the January 13, 2001 El Salvador earthquake (M_w 7.7), significant moment release
329 is observed along a steeply (60°) dipping plane with a down-dip dimension of roughly 25
330 km, extending well into the subducted upper mantle (Vallée et al., 2003).

The maximum depth of intraslab seismicity is well known to correlate with slab thermal parameter, the product of slab age and subduction rate (Kirby et al., 1996). This is commonly interpreted to reflect the temperature-dependant locus of dehydration within metamorphosed oceanic crust and serpentinized slab mantle (Raleigh and Paterson, 1965; Peacock, 2001; Hacker et al., 2003a,b). However, MCS observations also show that the dense and deep-cutting faulting of the older (14-24 Ma), colder and thicker (50-55 km) downgoing Cocos plate at the Middle America trench provides a mechanism to embed into the oceanic plate a volume of water much greater than that for the young (4-10 Ma), warm and thin (30-35 km) Juan de Fuca plate. This enhanced availability of water may create an environment more prone to brittle failure once the dehydration processes start. Moreover, water bound within the Cascadia slab is mostly contained within the hydrous crustal mineral phases, rather than serpentinized mantle peridotite, which remains stable at higher temperatures (greater depths) within the slab (Yamasaki and Seno, 2003; Hacker et al., 2003b). Deep fault penetration into the Cocos plate at the Middle America trench also creates pre-existing zones of weakness with larger surface area relative to those at the Cascadia margin, leading to higher potential for larger magnitude intraslab earthquakes.

In addition to the low frequency of intraslab earthquakes beneath Cascadia, relative to Middle America, we note that the sparse seismicity of the slab is clustered tightly within the northern and southern portions of the plate (Fig. 1). The uniform thickness and structure of Juan de Fuca crust formed along the spreading center (Nedimović, et al., 2005) suggests that these clusters may be caused by anomalous hydration of the lithospheric plate as it ages and/or by larger intraslab differential stresses. In this regard, the northward migration of the Mendocino Triple Junction and the accompanying retreat of the slab (Furlong and Schwartz, 2004) may create anomalous stress conditions along the southern margin of the plate. The Mendocino transform zone

357 also may be cooled more rapidly than the rest of the plate due to a thermal boundary
358 effect (e.g., Louden and Forsyth, 1976) caused by juxtaposition of the old and cold
359 Pacific plate and the young and warm Gorda plate, allowing deeper and more extensive
360 hydration along this long-lived fault zone. Further facilitating hydration of the oceanic
361 plate in this area are two sets of crossing faults observed in reflection profiles (Gulick et
362 al., 2001). The internally deforming and fragmenting southern Gorda plate is rotating
363 clockwise toward the Mendocino triple junction. This causes the incoming ridge fabric to
364 be oriented at a high angle to the trench (Fig. 1). When the strike of the incoming oceanic
365 spreading fabric forms an oblique angle (>20-30°) with the trench, a new set of trench-
366 parallel faults is formed (Masson, 1991) providing fluid pathways into the oceanic plate
367 in addition to those formed at the spreading center and reactivated near the trench.

368 In the north, intraslab stresses are influenced by interactions with the Nootka
369 transform fault, which plunges beneath mid-western Vancouver Island (Fig. 1), and by
370 the sharp along-strike bending of the slab beneath Olympic Peninsula. The trench bends
371 westward in this area and, like at the southern Gorda plate, becomes oblique to the ridge
372 tectonic fabric. Therefore, it is possible that two-directional faulting and associated
373 enhanced plate hydration also take place in this northern locality but without new MCS
374 data this cannot be validated.

375 **6. Effect of propagator wakes**

376 We also investigate the spatial relationship between the location of propagator
377 wakes and the distribution of seismicity within both the Juan de Fuca plate system and
378 the subducted oceanic slab at the Cascadia margin. While the smaller Explorer and
379 Gorda plates show evidence of seismicity, and presumably active faulting, throughout
380 much of their interior [e.g., Fox and Dziak, 1999; Dziak, 2006], earthquakes located
381 within the Juan de Fuca plate are concentrated along a broad NE-trending propagator

wake crossing the eastern Cleft ridge flank (Fig. 1). This region includes a swarm of >600 SOSUS-detected events recorded in April 2008, positioned near 44°N/128°W (Figs. 1 and 5). The affected area is located near the eastern end of our seismic transect 87-89-73-89a. Analysis of the seismic reflection image formed along this 300 km-long transect shows that the only observable faulting in this profile spans the area crossing this propagator wake (Fig. 6). These observations suggest that propagator wakes, as potential zones of plate weakness inherited from crustal accretion, may respond to increasing external stresses by brittle failure earlier and to a greater extent than other parts of oceanic plates. Therefore, the identified faulting and associated earthquake activity indicate that propagator wakes also may be areas of more pervasive plate hydration. As such, these structures should after subduction correlate with zones of elevated intraslab seismicity, assuming that dehydration embrittlement is an important mechanism for triggering intermediate-depth earthquakes within the subducting slab.

Analysis of Fig. 1, however, shows that at the Cascadia margin there does not appear to be a regional correlation between the inferred location of propagator wakes within the subducted oceanic slab and the location of anomalous intraslab seismicity. Despite the increased faulting of the Juan de Fuca plate along the propagator wakes, high temperatures within this young and sedimented oceanic plate may generally limit hydration of even the uppermost mantle such that additional hydration of the propagator areas is limited in volume.

Locally, on the other hand, the propagator wake inferred beneath Olympic Peninsula does appear to spatially correlate with the largest concentration of intraslab seismicity at the northern Cascadia margin. Magnetic isochrons (Fig. 1) suggest that the oceanic plate in this area may be older than in any other section of the subducted Juan de Fuca plate system found at about the same distance from the trench. Taking into account the N-S variability in the recent Cascadia margin convergence rates (e.g., 29 mm/yr at the

Oregon-Washington border, 40 mm/yr at the Juan de Fuca Strait; Wells et al., 2002), this section of the subducted plate exhibiting intraslab seismicity was likely the oldest and therefore the coldest when it was at the trench. This, combined with additional fluid pathways within the propagator wake area, likely facilitated deeper and more extensive mantle hydration than elsewhere in the subduction zone and may contribute to the locally elevated intraslab seismicity rate.

7. Summary

MCS data from EW0207 cruise provide the first direct imagery showing crustal scale faulting within the Juan de Fuca plate. Steeply dipping faults within the sedimentary layering are identified by stratigraphic offsets, with dip slip motion decreasing upsection. Imaged faults are generally spatially tied to larger offset scarps in the basement topography, suggesting reactivation of the normal fault systems formed at the spreading center. The analysis of EW0207 data, combined with reflection images within the area from earlier data, was used to map the extent of the Juan de Fuca plate region affected by normal faulting. The mapped region of recent faulting appears to extend to distances of >200 km from the trench.

Imaged reflections within the gabbroic igneous crust indicate swallowing fault dips at depth. These reflections require local alteration to produce an impedance contrast, suggesting that these structures provide pathways for fluid transport and hydration. As the depth extent of imaged faulting within this young and sediment insulated oceanic plate is primarily limited to approximately Moho depths (temperatures reach 500-600 °C), fault-controlled hydration is for the most part restricted to crustal levels. Hydration of a thin layer of the uppermost mantle is most likely for sections along the trench where the coldest and anomalously faulted parts of the Juan de Fuca plate system are subducted. If dehydration embrittlement is an important mechanism for triggering intermediate-

433 depth earthquakes within the subducting slab, then the limited occurrence rate and
434 magnitude of intraslab seismicity at the Cascadia margin may in part be explained by the
435 limited amount of water imbedded into the uppermost oceanic mantle prior to subduction.

436 The distribution of earthquakes within the Juan de Fuca plate system, including the
437 2008 earthquake swarm, indicates that propagator wake area is likely to be more heavily
438 faulted and therefore more hydrated than other parts of oceanic plates. However, being
439 mostly restricted to the crust, this additional hydration does not appear to have an effect
440 on the distribution and magnitude of the intraslab seismicity at the Cascadia margin
441 except, perhaps, for the anomalous area below the Olympic Peninsula.

Acknowledgements

This work was made possible through the generosity of American (T. M. Brocher, J. B. Diebold, A. M. Trehu), Canadian (K. Vasudevan) and German (E. Flueh, D. Klaeschen) researchers who provided seismic reflection data. D. S. Wilson kindly supplied magnetic isochron information and critically reviewed the manuscript. We are grateful to M. Protti, L. R. Sykes and G. A. Abers for comments on earlier drafts of this work, which was supported by the Doherty Foundation and the National Science Foundation under grants OCE002488 and OCE0648303 to SMC and MRN.

References

Brocher, T.M., Davis, M.J., Clarke, S.H., Geist, E.L., 1995. Onshore-offshore wideangle seismic recordings in October 1994 near Cape Blanco, Oregon. U.S. Geological Survey Open-File Report 95-819, 69 p.

Calvert, A.J., Clowes, R.M., 1991. Seismic evidence for the migration of fluids within the accretionary complex of western Canada. Can. J. Earth Sci. 28, 542-556.

Calvert, A.J., 1996. Seismic reflection constraints on imbrication and underplating of the northern Cascadia convergent margin. Can. J. Earth Sci. 33, 1294-1307.

Chaytor, J.D., Goldfinger, C., Dziak, R.P., Fox, C.G., 2004. Active deformation of the Gorda "Plate": Constraining deformation models with new geophysical data. Geology 32, 353-356.

Davis, E.E., Karsten, J.L., 1986. On the cause of the asymmetric distribution of seamounts about the Juan de Fuca Ridge; ridge-crest migration over a heterogeneous asthenosphere. Earth Planet. Sci. Lett. 79, 385-396.

Dziak, R.P., 2006, Explorer deformation zone: Evidence of a large shear zone and reorganization of the Pacific-Juan de Fuca-North American triple junction, Geology, 34, 312-316.

Flueh, E.R., Fisher, M.A., Bialas, J., Childs, J.R., Klaeschen, D., Kukowski, N., Parsons, T., Scholl, D.W., ten Brink, U., Trehu, A.M., Vidal, N., 1998. New seismic images of the Cascadia subduction zone from cruise SO108 – ORWELL. Tectonophysics 293, 69-84.

Fox, C.G., Dziak, R.P., Matsumoto, H., Schreiner, A.E., 1994. Potential for monitoring low- level seismicity on the Juan de Fuca Ridge using fixed hydrophone arrays. Mar. Tech. Soc. J. 27, 22–30.

Fox, C. G., and R. P. Dziak, 1999. Internal deformation of the Gorda Plate observed by hydroacoustic monitoring. J. Geophys. Res. 104, 17603-17616.

476 Furlong, K. P., S. Y. Schwartz, 2004. Influence of the Mendocino triple junction on the
477 tectonics of coastal California. Annual Review of Earth and Planetary Sciences, 32,
478 403-433.

479 Gulick, S.P.S., Meltzer, A.S., Clarke, S.H. Jr., 1998. Seismic structure of the southern
480 Cascadia subduction zone and accretionary prism north of the Mendocino triple
481 junction. J. Geophys. Res. 103, 27207- 27222.

482 Gulick, S. P. S., Meltzer, A. S., Henstock, T. J., Levander, A., 2001. Internal deformation
483 of the southern Gorda plate: Fragmentation of a weak plate near the Mendocino triple
484 junction, Geology, 29, 691-694.

485 Hacker, B.R., Abers, G.A., Peacock, S.M., 2003a. Subduction factory: 1. Theoretical
486 mineralogy, densities, seismic wave speeds, and H_2O content. J. Geophys. Res. 108,
487 B12029, doi:10.1029/2001JB001127.

488 Hacker, B. R., S. M. Peacock, G. A. Abers, and S. D. Holloway, 2003b. Subduction
489 factory: 2. Are intermediate-depth earthquakes in subducting slabs linked to
490 metamorphic dehydration reactions? J. Geophys. Res. 108, B12030,
491 doi:10.1029/2001JB001129.

492 Harris, R.N., Wang, K., 2002. Thermal models of the Middle America Trench at the
493 Nicoya Peninsula, Costa Rica. Geophys. Res. Lett. 29, 21-24.

494 Hyndman R.D., Wang, K., 1993. Thermal constraints on the zone of major thrust
495 earthquake failure: The Cascadia subduction zone. J. Geophys. Res. 98, 2039-2060.

496 Hyndman, R.D., Wang, K., 1995. The rupture of Cascadia great earthquakes from current
497 deformation and thermal regime. J. Geophys. Res. 100, 22133-22154.

498 Jung, H., Green, H.W.II, Dobrzhinetskaya, L.F., 2004. Intermediate-depth earthquake
499 faulting by dehydration embrittlement with negative volume change. Nature 428,
500 545-549.

501 Kao, H., Wang., K., Chen, R.Y., Wada, I., He, J., Malone, S.D., 2008. Identifying the
502 rupture plane of the 2001 Nisqually, Washington, Earthquake. Bull. Seis. Soc. Am.
503 98, doi:10.1785/0120070160, 1546-1558.

504 Kirby, S., Engdahl, R.E., Denlinger, R., 1996. Intermediate-depth intraslab earthquakes
505 and arc volcanism as physical expressions of crustal and uppermost mantle
506 metamorphism in subducting slabs, in: Bebout, G.E., Scholl, D., Kirby, S., Platt, J.P.
507 (Eds.), Subduction: Top to Bottom. Geophysical Monograph 96, American
508 Geophysical Union, Washington DC, pp. 195-214.

509 Kodaira, S., Iidaka, T., Kato, A., Park, J.-O., Iwasaki, T., Kaneda, Y., 2004. High pore
510 fluid pressure may cause silent slip in the Nankai Trough. Science 304, 1295–1298.

511 Louden, K.E., Forsyth, D.W., 1976. Thermal conduction across fracture zones and the
512 gravitational edge effect. J. Geophys. Res. 81, 4869-4874.

513 MacKay, M.E., Moore, G.F., Cochrane, G.R., Moore, J.C., Kulm, L.D., 1992. Landward
514 vergence and oblique structural trends in the Oregon margin accretionary prism:
515 Implications and effect on fluid flow. Earth Planet Sci. Lett. 109, 477-491.

516 Malone, S., 2001. Preliminary report on the Mw=6.8 Nisqually,Washington, earthquake
517 of 28 February 2001. Seism. Res. Lett. 72, 352–361.

518 Masson, D.G., 1991. Fault patterns at outer trench walls. Mar. Geophys. Res. 13, 209-
519 225.

520 McCrory, P.A., Blair, J.L., Oppenheimer, D.H., Walter, S.R., 2004. Depth to the Juan De
521 Fuca Slab Beneath the Cascadia Subduction Margin – A 3-D Model for Sorting
522 Earthquakes. U.S. Geological Survey Data Series 91, version 1.0.

523 Meade, C., Jeanloz, R., 1991. Deep-focus earthquakes and recycling of the water into the
524 earth's mantle. Science 252, 68-72.

525 Moore, J.C., Vrolijk, P., 1992. Fluids in accretionary prisms. Rev. Geophys. 30, 113-135.

526 Nedimović, M.R., Hyndman, R.D., Ramachandran, K., Spence, G.D., 2003a. Reflection
527 signature of seismic and aseismic slip on the northern Cascadia subduction interface.
528 Nature 424, 416-420.

529 Nedimović, M.R., Mazzotti, S., Hyndman, R.D., 2003b. Three-dimensional structure
530 from feathered two-dimensional seismic reflection data; The eastern Nankai trough.
531 J. Geophys. Res. 108, B10, 2456, doi:10.1029/2002JB001959, 1-14.

532 Nedimović, M.R., Carbotte, S.M., Harding, A.J., Detrick, R.S., Canales, J.P., Diebold,
533 J.B., Kent, G.M., Tischer, M., Babcock, J.M., 2005. Frozen magma lenses below the
534 oceanic crust. Nature 436, 1149-1152.

535 Nedimović, M. R., Carbotte, S. M., Diebold, J. B., Harding, A. J., Canales, J. P., Kent, G.
536 M., 2008. Upper crustal evolution across the Juan de Fuca ridge flanks. Geochem.
537 Geophys. Geosyst., 9, Q09006, doi:10.1029/2008GC002085, 1-23.

538 Oleskevich, D.A., 1996. Thermal constraints on great earthquake rupture zones [M.Sc.
539 Thesis]: University of Victoria, 170 p.

540 Peacock, S.M., 1990. Fluid Processes in Subduction Zones. Science 248, 329-337.

541 Peacock, S.M., 2001. Are the lower planes of double seismic zones caused by serpentine
542 dehydration in subducting oceanic mantle? Geology 29, 299-302.

543 Raleigh, C.B., Paterson, M.S., 1965. Experimental deformation of serpentinite and its
544 tectonic implications. J. Geophys. Res. 70, 3965-3985.

545 Ranero, C. R., Phipps Morgan, J., McIntosh, K., Reichert, C.B., 2003. Bending-related
546 faulting and the mantle serpentinization at the Middle America trench. Nature 425,
547 367-373.

548 Rogers, G.C., Crosson, R.S., 2002. Intraslab earthquakes beneath Georgia Strait/Puget
549 Sound, in: Kirby, S., Wang, K., Dunlop, S., (Eds.), The Cascadia Subduction Zone
550 and Related Subduction Systems. U.S. Geological Survey Open-File Report 02-328
551 and Geological Survey of Canada Open-File 4350, pp. 65-68.

552 Seno, T., Yoshida, M., 2004. Where and why do large shallow intraslab earthquakes
553 occur? Physics of Earth and Planetary Interiors 141, 183-206.

554 Shipley, T.H., Moore, G.F., Bangs, N.L., Moore, J.C., Stoffa, P.L., 1994. Seismically
555 inferred dilatancy distribution, northern Barbados Ridge decollement: Implications
556 for fluid migration and fault strength. Geology 22, 411-414.

557 Tatsumi, Y., Eggins, S., 1995. Subduction zone magmatism, Oxford, Blackwell Science.

558 Ulmer, P., Trommsdorff, V., 1995. Serpentine stability to mantle depths and subduction-
559 related magmatism. Science 268, 858-861.

560 Underwood, M.B., Hoke, K.D., Fisher, A.T., Davis, E.E., Giambalvo, E., Zühlsdorff, L.,
561 Spinelli, G.A., 2005. Provenance, stratigraphic architecture, and hydrogeologic
562 influence of turbidites on the mid-ocean ridge flank of northwestern Cascadia Basin,
563 Pacific Ocean. J. Sediment. Res. 75, 149–164.

564 Vallée, M., M. Bouchon, S.Y. Schwartz, 2003, The 13 January 2001 El Salvador
565 earthquake: A multidata analysis, J. Geophys. Res., 108, 2203,
566 doi:10.1029/2002JB001922.

567 Wada, I., Wang, K., He., J., Hyndman, R.D., 2008. Weakening of the subduction
568 interface and its effects on surface heat flow, slab dehydration, and mantle wedge
569 serpentinization. J. Geophys. Res. 113, B04402, doi:10.1029/2007JB005190.

570 Wang, K., Mulder, T., Rogers, G.C., Hyndman, R.D., 1995. Case for very low coupling
571 stress on the Cascadia subduction fault. J. Geophys. Res. 100, 12907-12918.

572 Wang, K., He, J., Davis, E.E., 1997. Transform push, oblique subduction resistance, and
573 intraplate stress of the Juan de Fuca plate. J. Geophys. Res. 102, 661-674.

574 Wang, K., Cassidy, J.F., Wada, I. Smith, A.J., 2004. Effects of metamorphic crustal
575 densification on earthquake size in warm slabs. Geophys. Res. Lett. 31, L01605,
576 doi:10.1029/2003GL018644.

577 Wells, R.E., Blakely, R.J., Weaver, C.S., 2002. Cascadia microplate models and within-
578 slab earthquake, in: Kirby, S., Wang, K., Dunlop, S., (Eds.), The Cascadia
579 Subduction Zone and Related Subduction Systems. U.S. Geological Survey Open-
580 File Report 02-328 and Geological Survey of Canada Open-File 4350, pp. 17-23.

581 Wilson, D.S., 1988. Tectonic history of the Juan de Fuca ridge over the last 40 million
582 years. J. Geophys. Res. 93, 11863-11876.

583 Wilson, D.S., 1993. Confidence intervals for motion and deformation of the Juan de Fuca
584 plate. J. Geophys. Res. 98, 16053-16071.

585 Wilson, D.S., 2002. The Juan de Fuca plate and slab—Isochron structure and Cenozoic
586 plate motions, in: Kirby, S., Wang, K., Dunlop, S., (Eds.), The Cascadia Subduction
587 Zone and Related Subduction Systems. U.S. Geol. Survey Open-File Report 02-328
588 and Geological Survey of Canada Open-File 4350, pp. 9-12.

589 Wong, I.G., 2004. Low potential for large intraslab earthquakes in the central Cascadia
590 subduction zone: Bull. Seis. Soc. Am., 95, 1880-1902.

591 Yamasaki, T., and T. Seno, 2003. Double seismic zone and dehydration embrittlement of
592 the subducting slab. J. Geophys. Res. 108, B42212, doi:10.1029/2002JB001918.
593

Figure captions

Fig. 1. Juan de Fuca plate regional seismicity and crustal age superimposed over grayscale bathymetry. Crustal scale marine MCS profiles from eight regional surveys are shown using thick brown lines. Line numbers are defined as in original surveys. White sections on transects 17-3-1, 34-32 and 87-89-73-89a represent the locations of the images shown in Figs. 2, 3, 4 and 6 respectively. Dashed white rectangle outlines the area shown in Fig. 5. Thick dashed orange line shows the location of the thermal profile of Wang et al. (1995) crossing the northern Cascadia margin. Thick black line on the subducting plates outlines the seaward limit of the region of extension or transtension where normal faulting is observed (solid) or inferred (dashed). Doted black line shows the location of the trench. Long N-trending black isodepth lines (McCrory et al., 2004) show the position of the Juan de Fuca oceanic slab beneath North America. Red dots are earthquakes recorded from 1991 to 2004 by the Sound Surveillance System (SOSUS) (Fox et al., 1994; http://www.pmel.noaa.gov/vents/acoustics/autochart/GetPosit.html). Blue dots are intraslab earthquakes with magnitudes >2 recorded from 1975 to 2002 and extracted from the Advanced National Seismic System catalog (McCrory et al., 2004). Green dots near the eastern end of transect 87-89-73-89a represent the SOSUS-detected earthquake swarm from April 2008. White lines with black edges are the interpreted traces of the ridge axis; dashed over fracture zones. Thin pink lines are magnetic isochrons that outline color shaded magnetic anomalies 1 through 5C, and grey shading outlines propagator wakes (Wilson, 1988; 2002). JDF – Juan de Fuca plate; EX – Explorer plate; GA – Gorda deformation zone; RDFZ – Revere-Dellwood fracture zone; SFZ – Sovanco fracture zone; NF – Nootka fault; BFZ – Blanco fracture zone; MFZ – Mendocino fracture zone. Inset in the upper right corner shows the location of the study area with respect to North America.

Fig. 2. Seismic reflection image of normal faults rooted near the Moho discontinuity and extending through the crust and the overlying sediments is extracted from transect 17-3-1 (see Fig. 1 for location). Such direct imaging of normal faulting in young oceanic plates from seafloor to Moho is not common because normal-fault planes dip steeply and generally appear transparent for the seismic reflection method. Temperatures on the right side are derived from a half-space cooling model for 2.75 Ma-old oceanic crust assuming thermal diffusivity $\kappa=0.804 \times 10^{-6}$ m^2/s and initial temperature $T_m=1300$ °C. To simulate the impact of sedimentation, the temperature at the sediment-basement interface is constrained as $T_s=25$°C, which assumes an average sediment thickness of 250 m as plate ages and a 0.1 °C/m thermal gradient in the sediments. Advanced 1D and 2D finite-element models of Juan de Fuca plate temperatures for areas closer to the trench and within the subduction zone can be found in Wang et al. (1995) and Hyndman and Wang (1993, 1995).

Fig. 3. Seismic reflection images showing normal faulting within the sediments at the eastern end of transect 34-32. Also visible in the sections are the igneous basement reflection and the layer 2A/2B event that is believed to mark the location of the upper crustal interface between the extrusives and sheeted dikes. (a) An 80 km-long section of transect 34-32 (see Fig. 1 for location) depicting the gradual westward transition from faulted to not faulted sediments. The white dashed box in (a) outlines the location of the detailed image of faulting shown in depth in (b). Conversion from twtt to depth was done along vertical rays using interval velocities. The discontinuity marked by a vertical white line in (b) at the distance of ~129 km is at the location where lines 34 and 32 were merged.

Fig. 4. Reflection image of the section of transect 17-3-1 showing significant sediment accumulation confined to mini-basins found on the western Endeavour ridge flank.

643 Folding of sedimentary strata due to differential compaction over the rough igneous
644 basement is present throughout the mini-basins, but no faulting can be observed although
645 the steps in the basement reach up to a few hundred meters.

646 Fig. 5. Earthquake swarm of 2008 (red dots) superimposed over crustal age and grayscale
647 bathymetry of the Cleft ridge segment (see Fig. 1 for location). Orange solid line is MCS
648 transect 87-89-73-89a from the EW0207 cruise. Reflection image of the transect section
649 underlined with a thick solid white line is shown in Fig. 6.

650 Fig. 6. Seismic reflection image showing the approximate location of the landward onset
651 of faulting at the eastern end of transect 87-89-73-89a (see Figs. 1 and 5 for location).
652 The earthquake swarm shown in Fig. 5 partially overlaps the faulted section and extends
653 further east.

654 **Table captions**

655 Table. 1. Summary information characterizing seismic reflection data from all crustal
656 scale MCS surveys with streamers 2.4 km or longer across the Juan de Fuca plate system.

Nedimovic et al., Fig. 1

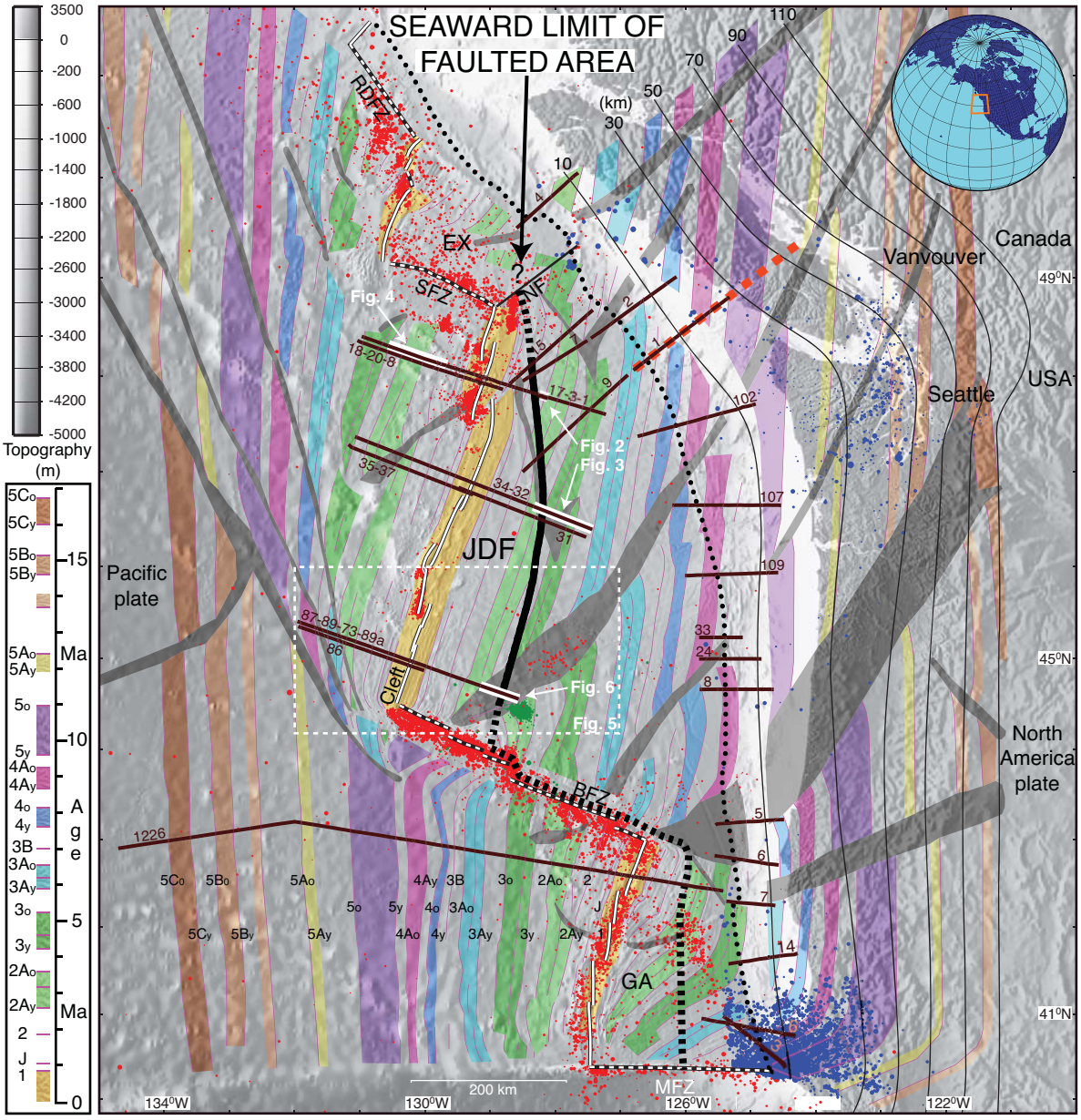

Nedimovic et al., Fig. 2

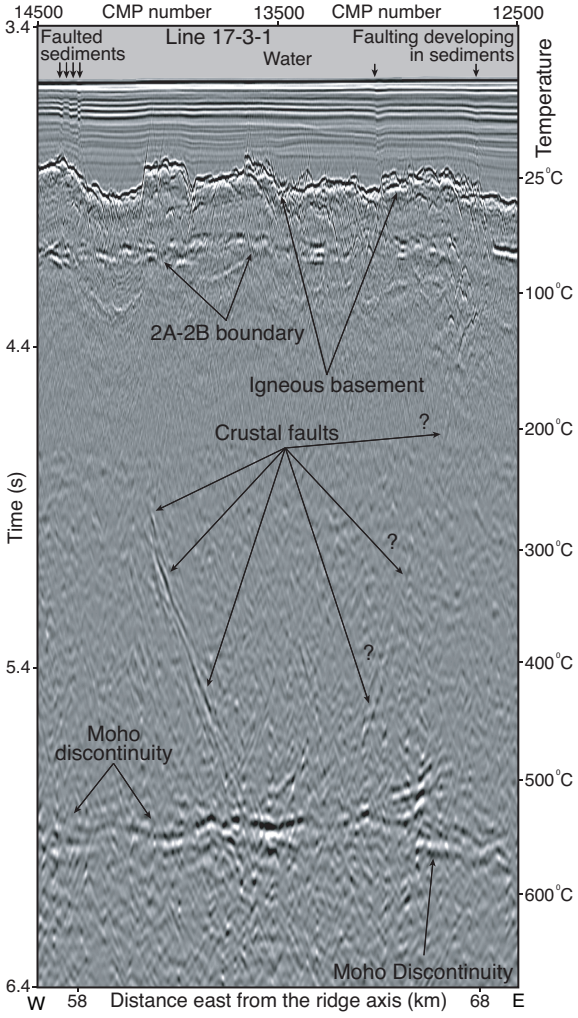

Nedimovic et al., Fig. 3

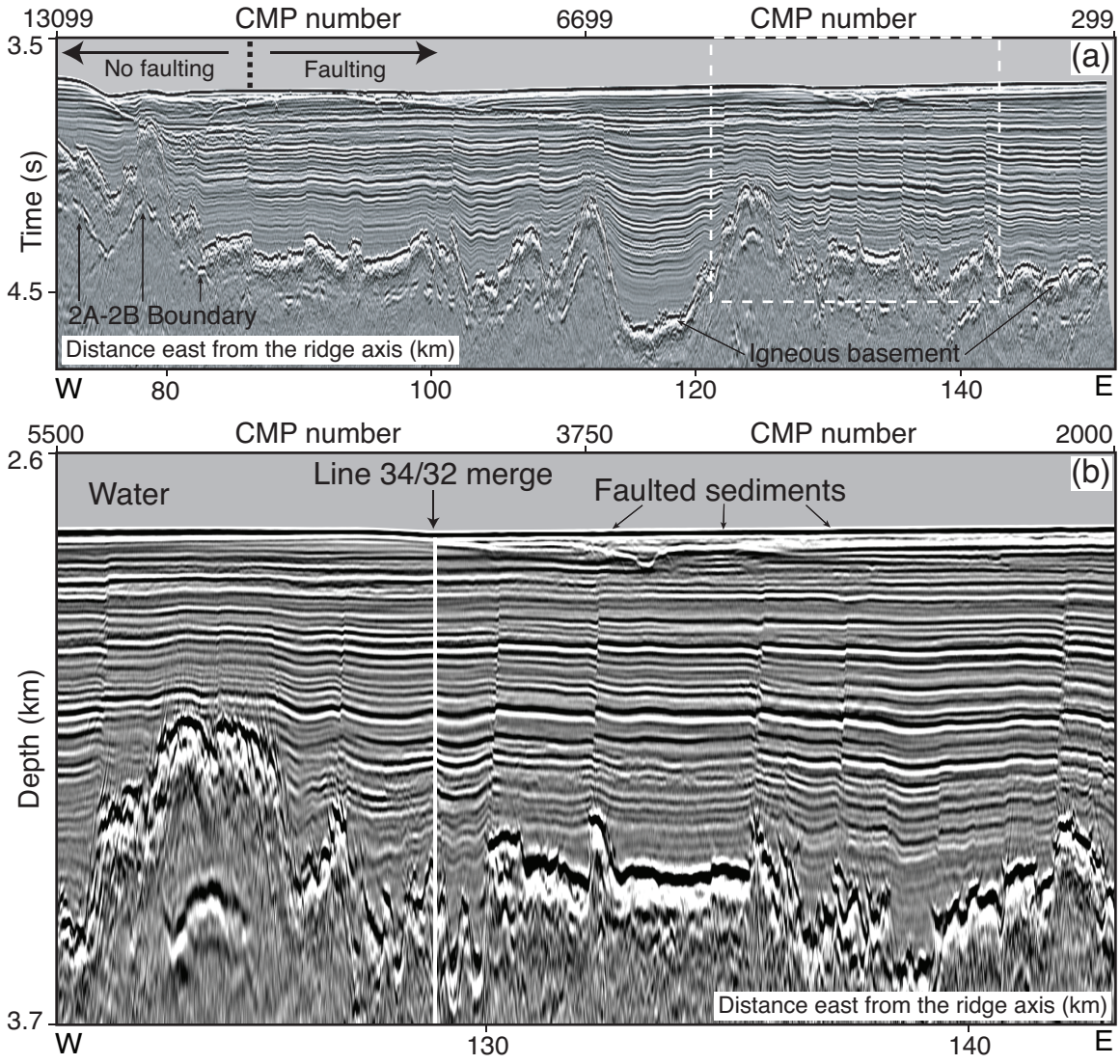

Nedimovic et al., Fig. 4

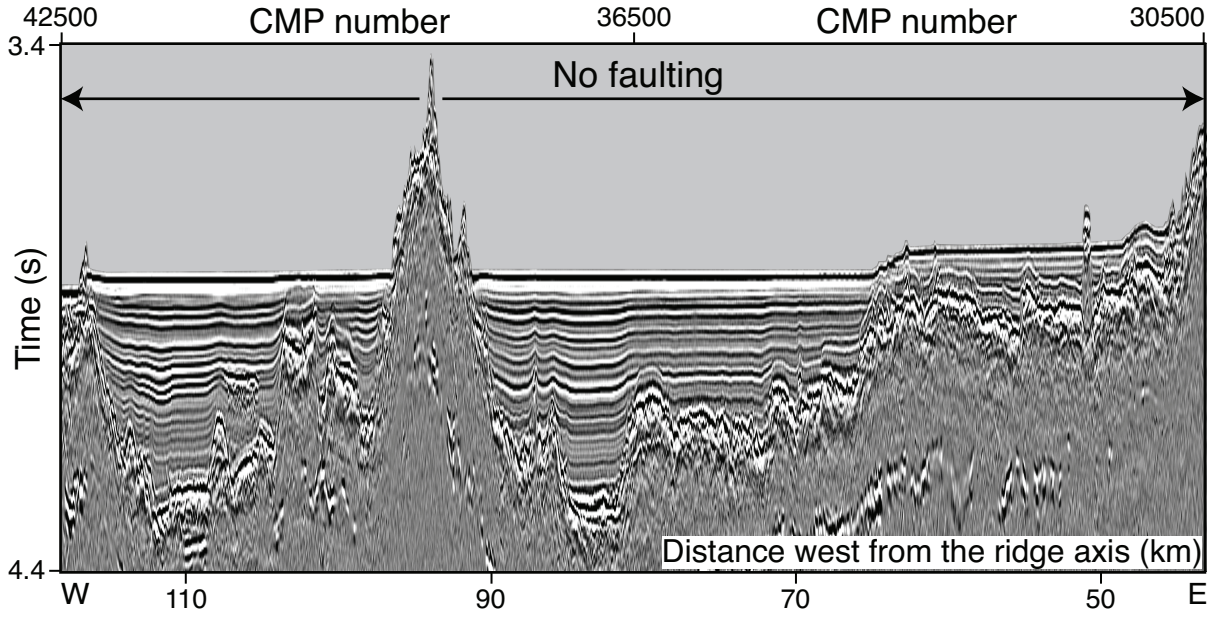

Nedimovic et al., Fig. 5

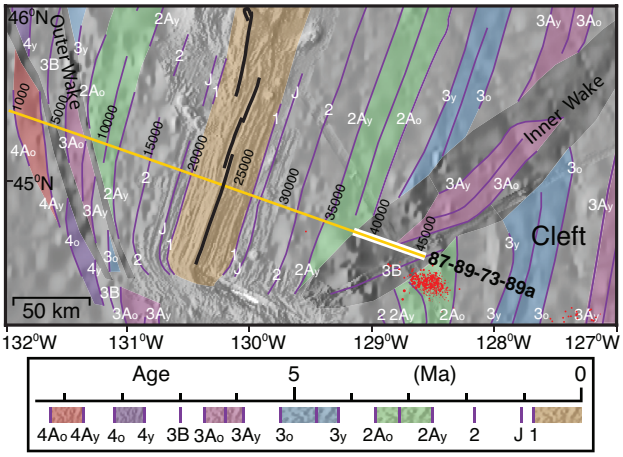

Nedimovic et al., Fig. 6

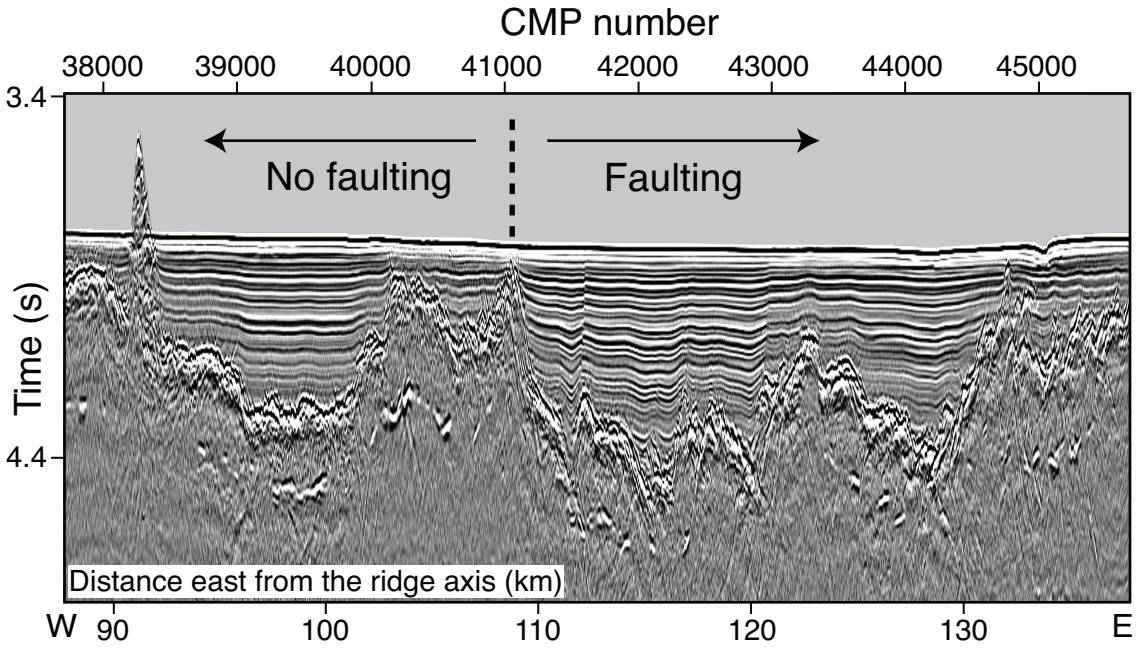

Project name & year	Profiles used in this study	Streamer length & type	Channels: number & spacing	Airgun array & volume	Shot spacing	Record length & sample rate	CMP spacing & fold	References
Juan de Fuca, EW0207 (2002)	17-3-1, 18-20-8, 34-32, 35-37, 31, 87-89-73-89a, 86	6 km, digital	480, 12.5 m	10-element, 49.2 L	37.5 m	10.24 s, 2 ms	6.25 m, 80	Nedimovic et al., 2005
Canadian Frontier Geoscience Project (1985)	1, 2, 4, 7, 9	3 km, analogue	120, 25 m	108.3 L	50 m	16 s, 4 ms	12.5 m, 30	Calvert and Clowes, 1991
ODP Leg 146 site survey, Vancouver Island (1989)	15	3.6 km, analogue	144, 25 m	128.2 L	50 m	16 s, 4 ms	12.5 m, 36	Calvert, 1996
ODP Leg 146 site survey, offshore Oregon (1989)	8, 24, 33	3.6 km, analogue	144, 25 m	128.2 L	25 m	8 s, 4 ms	12.5 m, 72	MacKay et al., 1992
Orwell Project, SOONE SO108 (1996)	102, 107, 109	2.4 km, analogue	48, 50 m	87.4 L	50 m	16 s, 4 ms	25 m, 24	Flueh et al., 1998
Gorda Rise EW9413 (1994)	1226	4 km, digital	160, 25 m	20-element, 137.5 L	50 m	12 s, 2 ms	12.5 m, 40	*UTIG web pages
Cape Blanco, EW9414 (1994)	5, 6, 7	4 km, digital	160, 25 m	10-element, 49.2 L	50 m	14 s, 2 ms	12.5 m, 40	Brocher et al., 1995
Mendocino Triple Junction, EW9407 (1994)	3, 6, 14	4 km, digital	160, 25 m	10-element, 49.2 L	50 m	14 s, 2 ms	12.5 m, 40	Gulick et al., 1998

Table 1. Summary information characterizing seismic reflection data from all crustal scale MCS surveys with streamers 2.4 km or longer across the Juan de Fuca plate system.

*http://www.ig.utexas.edu/sdc/cruise.php? cruiseIn=ew9413